UC Irvine
UC Irvine Previously Published Works

Title
Nonspatial sequence coding varies along the CA1 transverse axis

Permalink
https://escholarship.org/uc/item/6244j87n

Authors
Ng, Chi-Wing
Elias, Gabriel A
Asem, Judith SA
et al.

Publication Date
2018-11-01

DOI
10.1016/j.bbr.2017.10.015

Peer reviewed

eScholarship.org Powered by the California Digital Library
University of California

Nonspatial sequence coding varies along the CA1 transverse axis

Abbreviated Title: DISTRIBUTION OF SEQUENCE AND PLACE CODING IN CA1

Chi-Wing Ng[1], Gabriel A. Elias[1], Judith S.A. Asem[1], Timothy A. Allen[2], Norbert J. Fortin[1]

[1]Center for the Neurobiology of Learning and Memory, Department of Neurobiology and Behavior, University of California Irvine, Irvine, CA 92697

[2]Department of Psychology, Florida International University, Miami, FL 33199

Number of figures: 4
Number of tables: 1
Number of text pages: 25
Total Word Count: 9911

Corresponding Author:

Norbert J. Fortin, Ph.D.
Center for the Neurobiology of Learning and Memory
Department of Neurobiology and Behavior
University of California, Irvine
106 Bonney Research Laboratory
Irvine, CA 92697-3800
tel: 949-824-9740
email: norbert.fortin@uci.edu

Conflicts of Interest: The authors declare no competing financial interests.

Acknowledgments:

This research was supported in part by the National Science Foundation (awards IOS-1150292 and BCS-1439267 to N.J.F.), National Institutes of Health (T32 DC-010775 support for G.A.E.; T32 AG-000096 support for J.S.A.A.), the Whitehall Foundation (award 2010-05-84 to N.J.F.), and the University of California, Irvine. We thank Kei Igarashi and members of the Fortin Lab for useful discussions on the present work.

ABSTRACT

The hippocampus plays a critical role in the memory for sequences of events, a defining feature of episodic memory. To shed light on the fundamental mechanisms supporting this capacity, we recently recorded neural activity in CA1 as rats performed a nonspatial odor sequence memory task. Our main finding was that, while the animals' location and behavior remained constant, a proportion of CA1 neurons fired differentially to odors depending on whether they were presented in or out of sequence (sequence cells). Here, we further examined if such sequence coding varied along the distal-to-proximal axis of the dorsal CA1 region (distal: toward subiculum; proximal: toward CA3). Differences in information processing along this axis have been suggested by recent anatomical and electrophysiological evidence that odor information may be more strongly represented in the distal segment, whereas spatial information may be more strongly represented in the proximal segment. Recorded neurons were grouped into four arbitrary sections of dorsal CA1, ranging from distal to proximal. We found that, although sequence cell coding was observed across the distal-to-proximal extent of CA1 from which we recorded, it was significantly higher in intermediate CA1, a region with more balanced anatomical input from lateral and medial entorhinal regions. More specifically, in that particular segment of CA1, we observed a significant increase in the magnitude of sequence coding of all cells, as well as in the sequential information content of sequence cells. Importantly, a different pattern was observed when examining the distribution of spatial coding from the same electrodes. Consistent with previous reports, our results suggest that spatial information was more strongly represented in the proximal section of CA1 (higher proportion of cells with place fields). These findings indicate that nonspatial sequence memory coding is not uniformly distributed along the transverse axis of CA1, and that this distribution does not simply follow the expected gradient based on the stimulus modality or the degree of spatial selectivity. Instead, the observed distribution suggests this form of sequence coding may be associated with convergent input from lateral and medial entorhinal regions, which is present throughout the proximodistal axis but higher in intermediate CA1.

INTRODUCTION

Considerable research indicates the hippocampus is critical to episodic memory, the ability to recall one's past experiences. More specifically, the hippocampus, which receives a strong convergence of input from cortical regions, is thought to play a key role in associating information about specific events with the spatial and temporal contexts in which they occurred (Eichenbaum et al., 2012; Allen and Fortin, 2013; Howard and Eichenbaum, 2015; Knierim, 2015). Consistent with this view, neurons in hippocampal subregion CA1 have shown selectivity for specific stimuli, spatial locations, as well as specific time periods or temporal relationships (e.g., Wood et al., 1999; MacDonald et al., 2011; Igarashi et al., 2014b; Allen et al., 2016). Importantly, these different coding properties may not be uniformly distributed within CA1, as distal CA1 (toward subiculum) is more strongly associated with the lateral entorhinal cortex (LEC) and proximal CA1 (toward CA3) with the medial entorhinal cortex (MEC; Witter et al., 2000; Naber et al., 2001; Igarashi et al., 2014a; Cappaert et al., 2015; Knierim, 2015).

Recent evidence suggests that distal CA1 and LEC are anatomically and functionally related and play a key role in supporting nonspatial forms of memory. Distal CA1 receives stronger projections from LEC than MEC, whereas proximal CA1 shows the opposite pattern (Witter et al., 2000; Naber et al., 2001; Honda et al., 2012; Cappaert et al., 2015). In addition, both distal CA1 and LEC neurons represent nonspatial attributes of experiences, such as the presentation of specific objects, odors, and other sensory stimuli (Knierim et al., 2006; Burke et al., 2011; Deshmukh and Knierim, 2011; Ito and Schuman, 2012; Igarashi et al., 2014b). The two regions also show functional coupling during behavior, in the form of highly coherent oscillations in the 20-40 Hz range (Igarashi et al., 2014b). Similarly, expression of the immediate early gene *Arc* is higher in distal than proximal CA1 during nonspatial recognition memory performance (Nakamura et al., 2013).

In contrast, accumulating evidence suggest the functional relationship between proximal CA1 and MEC is centered on the processing of spatial information. In fact, MEC neurons, which include grid cells, border cells, and head direction cells, provide dynamic mapping of the animal's location during navigation (Hafting et al., 2005; Sargolini et al., 2006; Solstad et al., 2008), whereas LEC neurons show weak spatial modulation (Hargreaves et al., 2005; Igarashi et al., 2014b). Relative to distal CA1 cells, place cells in proximal CA1 are more spatially selective, carry more spatial information, show higher rate remapping following changes to the environment, and exhibit stronger theta phase-coupling with spatially tuned MEC cells (Henriksen et al., 2010; Hartzell et al., 2013; Oliva et al., 2016). Relative to distal CA1, proximal CA1 also shows higher immediate early

gene (*c-fos*) activation during memory retrieval for spatially-cued contextual fear, and proximal (but not distal) CA1 lesions abolish such memory retrieval (Nakazawa et al., 2016).

Although this segregation in the representation of spatial and nonspatial event information along the transverse (proximodistal) axis of CA1 is compelling, it is unclear how information about the temporal context of events is distributed along the same axis. Is it more prevalent in distal CA1 because it is nonspatial information, or in proximal CA1 due to overlapping demands or computations with spatial information? Or does it exhibit a different pattern or gradient altogether? To address this issue, we re-examined a previously published dataset in which we recorded neural activity in hippocampal subregion CA1 as animals performed a nonspatial sequence memory task (Allen et al., 2016). In this task, rats received repeated presentations of odor sequences (e.g., ABCDE) at a single odor port and were required to identify each item as “in sequence” (e.g., AB<u>C</u>…) or “out of sequence” (e.g., AB<u>D</u>…). Our main finding was that a significant proportion of CA1 neurons fired differentially to items presented in or out of sequence (“sequence cells”) and that this form of sequence coding was linked to task performance. Critically, the recordings were performed from tetrodes that spanned much of the transverse axis of dorsal CA1 and included time periods in which the animal was traveling back and forth in the maze (between sequence presentations), thus providing a unique opportunity to directly compare the anatomical distribution of temporal (sequence) coding and spatial coding from the same set of electrodes. Specifically, we tested the hypothesis that neurons exhibiting nonspatial sequence coding (sequence cells) were not uniformly distributed along the transverse axis of CA1, and that their distribution was different than that of neurons exhibiting spatial coding (place cells).

MATERIALS AND METHODS

Neural activity was recorded from the transverse axis of dorsal CA1 as rats performed a cross-species, nonspatial sequence memory task recently developed in our laboratory (Allen et al., 2014, 2016; Figs 1, 2). Experimental procedures were reported in detail previously (Allen et al., 2016) and thus only summarized here. Briefly, the rat version of the task involves repeated presentations of sequences of nonspatial items (odors) and requires subjects to correctly identify each item as being presented "in sequence" (InSeq; by holding their response until the signal at 1.2 sec) or "out of sequence" (OutSeq; by withdrawing their response before the signal) to receive a water reward (Fig 1B). In the present study, we used five-item sequences and included two types of OutSeq probe trials (Repeats: e.g., AB<u>A</u>DE; Skips: e.g., A<u>D</u>CDE). In each session, a given odor sequence (e.g., Seq1: ABCDE) was presented 30–50 times, with approximately half of the presentations including all items InSeq (ABCDE) and half including one item OutSeq (e.g., AB<u>E</u>DE). Each odor presentation was initiated by a nose poke (provided 800 ms had elapsed since the previous odor) and was terminated after the rat either held for 1.2 sec (signaled by a beep) or pulled his nose out. Water rewards were delivered below the odor port after correct responses (10 µl) and at the opposite end of the track following correct completion of a full sequence (20 µl). Following an incorrect response, a buzzing sound was emitted, and the sequence was terminated. To enhance the segmentation between each odor sequence (completed correctly or not), rats were required to run to the end of the track opposite the odor port before the next sequence could be presented (Fig 1A), which allowed us to examine spatial coding properties in the same population of recorded neurons. To maximize our sample sizes, our analyses collapsed data from three separate sessions (Well-Trained, Novel1, and Novel2; see Allen et al., 2016), but data from a single session (Well-Trained) is also included for comparison.

Animals

Subjects were five male Long–Evans rats, weighing ~350 g at the beginning of the experiment. They were individually housed and maintained on a 12 h light/dark cycle. Rats had *ad libitum* access to food, but access to water was limited to 2–10 min each day, depending on how much water they received as reward during behavioral training (3–6 ml). On weekends, rats received full access to water for ≥12 h to ensure adequate overall hydration. Hydration levels were monitored daily. All procedures were conducted in accordance with the Institutional Animal Care and Use Committee.

Equipment and stimuli

The apparatus consisted of a linear track (length, 150 cm; width, 9 cm), with walls angled outward (30° from vertical; height, 40 cm). An odor port, located on one end of the track, was equipped with photobeam sensors to precisely detect nose entries and was connected to an automated odor delivery system capable of repeated deliveries of multiple distinct odors. Two water ports were used for reward delivery: one located under the odor port, the other at the opposite end of the track. Timing boards (Plexon) and digital input/output boards (National Instruments) were used to measure response times and control the hardware. All aspects of the task were automated using custom Matlab scripts (MathWorks). A 96-channel Multichannel Acquisition Processor (MAP; Plexon) was used to interface with the hardware in real-time and record the behavioral and electrophysiological data. Odor stimuli consisted of synthetic food extracts contained in glass jars (A, lemon; B, rum; C, anise; D, vanilla; E, banana; V, almond; W, cinnamon; X, coconut; Y, peppermint; Z, strawberry) that were volatilized with desiccated, charcoal-filtered air (flow rate, 2 L/min). To prevent cross-contamination, separate Teflon tubing lines were used for each odor. These lines converged in a single channel at the bottom of the odor port. In addition, an air vacuum located at the top of the odor port provided constant negative pressure to quickly evacuate odor traces. Readings from a volatile organic compound detector confirmed that odors were cleared from the port 500–750 ms after odor delivery (inter-odor intervals were limited by software to ≥800 ms).

Training

Naïve rats were initially trained to nosepoke and reliably hold their nose for 1.2 sec in the odor port for a water reward. Odor sequences of increasing length were then introduced in successive stages (A, AB, ABC, ABCD, and ABCDE) upon reaching behavioral criterion of 80% correct over three consecutive sessions per training stage. In each stage, rats were trained to correctly identify each presented item as either InSeq (by holding their nosepoke response until the signal at 1.2 sec to receive a water reward) or OutSeq (by withdrawing their nose before the signal to receive reward). There were two types of OutSeq items in the dataset: Repeats, in which an earlier item was presented a second time in the sequence (e.g., AB<u>A</u>DE), and Skips, in which an item was presented too early in the sequence (e.g., AB<u>D</u>DE, which skipped over item C). Although our previous work has revealed important differences in performance and neural activity on Repeats and Skips (Allen et al., 2014, 2015, 2016), this distinction was beyond the scope of the present analyses and not further discussed here. Note that OutSeq items could be presented in any sequence position except the first (i.e., sequences always began with odor A, though odor A could

also be presented later in the sequence as a Repeat). After reaching criterion performance on the five-item sequence (>80% correct on both InSeq and OutSeq items, over three consecutive sessions), rats underwent surgery for microdrive implantation.

Surgery

Rats received a preoperative injection of the analgesic buprenorphine (0.02 mg/kg, s.c.) ~10 min before induction of anesthesia. General anesthesia was induced using isoflurane (induction: 4%; maintenance: 1–2%) mixed with oxygen (800 ml/min). After being placed in the stereotaxic apparatus, rats were administered glycopyrrulate (0.5 mg/kg, s.c.) to help prevent respiratory difficulties. A protective ophthalmic ointment was then applied to their eyes, and their scalp was locally anesthetized with marcaine (7.5 mg/ml, 0.5 ml, s.c.). Body temperature was monitored and maintained throughout surgery and a Ringer's solution with 5% dextrose was periodically administered to maintain hydration (total volume of 5 ml, s.c.). The skull was exposed following a midline incision and adjustments were made to ensure the skull was level. Six support screws (four titanium, two stainless steel) and a ground screw (stainless steel; positioned over the cerebellum) were anchored to the skull. A piece of skull ~3 mm in diameter (centered on coordinates: −4.0 mm AP, 3.5 mm ML) was removed over the left hippocampus. Quickly after the dura was carefully removed, the base of the microdrive was lowered onto the exposed cortex, the cavity was filled with Kwik-Sil (World Precision Instruments), the ground wire was connected, and the microdrive was secured to the support skull screws with dental cement. Each tetrode was then advanced ~900 μm into the brain. Finally, the incision was sutured and dressed with Neosporin and rats were returned to a clean cage, where they were monitored until they awoke from anesthesia. One day following surgery, rats were given an analgesic (flunixin, 2.5 mg/kg, s.c.) and Neosporin was reapplied to the incision site.

Electrophysiological recordings

Each chronically implanted microdrive contained 20 independently drivable tetrodes. Following the surgical recovery period, tetrodes were slowly advanced over a period of ~3 weeks while monitoring established electrophysiological signatures of the CA1 pyramidal cell layer (e.g., sharp waves, ripples, and theta amplitude). Voltage signals recorded from the tetrode tips were referenced to a ground screw positioned over the cerebellum, and filtered for single-unit activity (154 Hz to 8.8 kHz). The neural signals were then amplified (10,000–32,000×), digitized (40 kHz), and recorded to disk with the data acquisition system (MAP, Plexon). Action potentials from individual neurons were manually isolated off-line using a combination of standard waveform

features across the four channels of each tetrode, interspike interval distributions for each isolated unit, and cross-correlograms for each pair of simultaneously recorded units on the same tetrode (Offline Sorter, Plexon). A total of 713 single units were recorded over 13 sessions (Well-Trained: *n* = 5 rats; Novel1: *n* = 4; Novel2: *n* =4). Units were classified as putative pyramidal neurons (n = 599) and interneurons (n = 114) by previously identified characteristic firing rates and valley-to-peak spike widths (Csicsvari et al., 1998, 1999; Mizuseki and Buzsáki, 2013; Allen et al., 2016), with both types of neurons included in our analyses. To confirm recording sites, current was passed through the electrodes before perfusion (0.9% PBS followed by 4% paraformaldehyde) to produce small marking lesions, which were subsequently localized on Nissl-stained tissue slices.

Tetrode placements along the transverse axis

Tetrodes were organized in a rectangular array along the mediolateral axis of CA1 (centered on -4.0 mm AP, with the long axis spanning approximately 2 mm – 5 mm ML). Recorded neurons were grouped according to their targeted section of the mediolateral axis of CA1 and divided into four medial-to-lateral sections (Fig 2), in which section 1 was the most medial (beginning at ~2 mm ML) and section 4 was the most lateral (ending at ~5 mm ML). Although the mediolateral and proximodistal axes are not directly aligned, our recordings sampled from the distal (section 1), intermediate (section 2, and part of section 3), and proximal (section 4, and part of section 3) extent of CA1 described in other studies (e.g., Henriksen et al., 2010; Oliva et al., 2016; though these studies had a more extensive sampling of distal CA1). Note that our objective was to match the CA1 boundaries described in these studies by using the thickening of the cell layer observed as CA1 transitions into CA2 (proximal boundary) or subiculum (distal boundary) as the main indicator. When this thickening of the cell layer was difficult to visualize on a particular slice (e.g., when the marking lesions obscured the boundary, as in Fig 2), we supplemented this information by using the location of the boundaries identified by Henriksen and colleagues (2010) in examples from corresponding slices.

Although the number of tetrodes was closely matched across the four sections, the number of tetrodes with isolated cells (sections 1 to 4: 12, 16, 13, 14) and the number of recorded cells (145, 233, 153, 182) were not identical. Therefore, the proportions of sequence cells or place cells reported were normalized to the total number of cells recorded in the corresponding section (see Table 1 for proportions for each animal). Importantly, expected values for the *G*-test were also normalized to the corresponding number of cells per section to control for differences in sampling. Finally, the ratios of putative pyramidal:interneuron cells recorded across the same four sections

were 5.3, 6.5, 5.1, and 4.2, and the average firing rates were 1.9 ± 0.38, 1.8 ± 0.27, 2.2 ± 0.51, 2.4 ± 0.38, and 2.1 ± 0.19.

Sequence coding analyses

Sequence cells. As described in our previous study (Allen et al., 2016), sequence cells are neurons that exhibit statistically significant differences in firing rate on InSeq vs OutSeq trials. These cells were identified using resampling, nonparametric statistics (Sokal and Rohlf, 1995; McKenzie et al., 2013; Neunuebel and Knierim, 2014), as spiking activity often violates the assumptions of normality and homogeneity of variance required for traditional (parametric) statistics. Spikes were binned into 50 ms bins, a bin size that helps capture potential firing rate dynamics within trials (e.g., bursting activity) during data visualization and analysis. However, to limit the number of statistical comparisons performed, only one statistical test was performed per 250 ms time window (*not* one test per 50 ms bin). For example, a *t* ratio was calculated for a given 250 ms time window by comparing all 50 ms bins from InSeq trials (five bins per time window * number of trials) to all 50 ms bins from OutSeq trials (five bins per time window * number of trials). Statistical significance was determined by estimating the probability of obtaining a *t* ratio this large (or larger) using *t* ratio distributions obtained by randomly permuting the 50 ms bins (across the two types of trials and the five bins; 1000 permutations). Since two 250 ms time windows were tested (-500 ms to –250 ms, -250 ms to 0 ms; relative to port withdrawal), we applied the Bonferroni correction, such that a comparison was considered statistically significant if this probability was < 0.025 (two-tailed). Note that the results presented hereafter were obtained using this random bin shuffling (as in Allen et al., 2016) but that, as a comparison, we also generated the distributions by permuting across trials only (preserving the order of the five bins within each trial) and observed nearly identical results (81 sequence cells, compared to 80 with the random bin permutations, with a 94.7% overlap in the cells identified), indicating that differences in activity were primarily accounted by trial type.

Note that this analysis excluded the first item of each sequence, as they were only presented InSeq. To match the overall proportions reported in our previous study (Allen et al., 2016), we combined the data from the three recording sessions and used the same conservative criterion to identify sequence cells. Under this conservative criterion, only OutSeq trials with odor sampling periods of at least 500 ms are included in the analyses, which excludes many correctly identified OutSeq trials, but ensures that differences are not simply due to limited sampling or to potential differences in internal motor dynamics or state immediately preceding the motor response (see Allen et al., 2016).

Sequential information content. To help quantify the degree to which sequence cells differentiated between InSeq and OutSeq items, we adapted previous measures of information content used in spatial (Skaggs et al., 1993) and temporal processing (MacDonald et al., 2013). As in Allen et al., (2016), the sequential information content (bits/sec) of each sequence cell was calculated using the following formula:

$$Sequential\ Information\ Content\ (bits/sec) = \left(P_{IN} \left(\frac{\lambda_{IN}}{\lambda}\right) log_2 \left(\frac{\lambda_{IN}}{\lambda}\right) + P_{OUT} \left(\frac{\lambda_{OUT}}{\lambda}\right) log_2 \left(\frac{\lambda_{OUT}}{\lambda}\right) \right) \times \lambda$$

where P_{IN} is the probability of an InSeq trial, P_{OUT} is the probability of an OutSeq trial, λ_{IN} is the firing rate of the cell during InSeq trials, λ_{OUT} is the firing rate of the cell during OutSeq trials, and λ is the overall mean firing rate of the cell during odor-sampling periods. Higher sequential information content values indicate greater differentiation in activity between InSeq and OutSeq items. Note that the maximum value would be 1 if the proportion of InSeq and OutSeq trials was identical, but since this is not the case here (OutSeq trials are much less frequent than InSeq trials) higher values can be observed (see Fig 3E).

Spatial coding analyses

Although spatial processing is not critical to performance of the odor sequence memory task, rats were required to run to the back of the apparatus to begin the next sequence presentation. This requirement, combined with occasional exploration of the environment, provided enough sampling to perform basic analyses of the spatial coding properties of individual neurons. Note that the place cell analysis included the whole maze but that the information content analysis was restricted to cells with place fields on the central runway, the section of the environment with the most consistent sampling (time spent in each pixel) and spatial behavior.

Place cells. Place cell analyses were consistent with that of previous studies (e.g., Henriksen et al., 2010; Lu et al., 2015; Oliva et al., 2016), with minor parameter adjustments due to the nature of our paradigm and apparatus. The animals' location in X-Y coordinates was recorded by a behavioral tracking system using headstage-fixed LEDs at a sampling rate of 30 Hz (CinePlex, Plexon). Using the NeuroExplorer software package (Nex Technologies), the environment was divided into pixels of 2.3 × 2.3 cm (i.e., 64 × 64 pixels) and firing rate maps were calculated for each unit (spikes per pixel over time spent in pixel; Gaussian filter width = 3). Pixels with insufficient sampling (< 1 sec time spent or < 15 visits) were assigned firing rate values of zero. Only units with at least 100

spikes and an average firing rate above 2 Hz were included in the analysis. Place fields were defined as a contiguous region of at least nine pixels, in which the firing rate of each pixel was at least 1.5 standard deviations above the average firing throughout the maze. Place cells were defined as cells with at least one place field with a field coherence above 0.01.

Spatial information content (runway only). To help quantify the amount of spatial information provided by each place cell, we calculated the spatial information content (bits/sec) as follows:

$$Spatial\ Information\ Content\ (bits/sec) = \left(\sum_i P_i \frac{\lambda_i}{\lambda} log_2 \frac{\lambda_i}{\lambda}\right) \times \lambda$$

where *i* is the pixel number, P_i is the probability of the occupancy (total time spent at pixel *i* divided by total time spent through the maze), λ_i is average firing rates of pixel *i*, and λ is the overall mean firing rate of the cell during the session (Skaggs et al., 1993).

Analyses comparing coding properties along the transverse axis

We examined the distribution of sequence and spatial coding along the transverse axis using several measures. Statistical comparisons involving numerical data (e.g., F ratios, information content) were performed using one-way ANOVAs, followed by posthoc tests comparing the section with the highest proportion with each of the other three sections (Sequence cells: 2vs1, 2vs3, 2vs4; Place cells: 4vs1, 4vs2, 4vs3; Holm-Sidak correction; Prism 6.0). Information content values were log-transformed for statistical analyses (because of positive skewness), but are displayed in raw values. Note that the same pattern of results was observed with nonparametric ANOVAs (Kruskal-Wallis one-way ANOVAs; Prism 6.0). Statistical comparisons involving proportions of cells across sections were performed using *G*-tests, which determined if the observed counts across sections were significantly different than expected by chance (i.e., even distribution). The *G*-test is a more robust alternative to the Chi-square test, especially for data sets including cells with smaller frequencies (Sokal and Rohlf, 1995). Analyses were considered statistically significant at $p < 0.05$.

RESULTS

Nonspatial sequence coding was not uniformly distributed along the CA1 transverse axis

The main objective of the present study was to test the hypothesis that the strength of nonspatial sequence coding varies along the proximodistal axis of CA1. Our previous study discovered that a significant proportion of CA1 neurons fired differentially to items presented InSeq or OutSeq (sequence cells; Allen et al., 2016; see examples in Fig 3A,B). Up to 26.2% of neurons active in the task (187 of 713) exhibited this coding property; however, the present analyses focused on the subset (11.2%; 80 of 713) that met the most stringent criterion described in Allen et al. (2016), which excluded trials with sampling windows shorter than 500 ms to control for potential differences in internal motor dynamics or state. Although most sequence cells fired preferentially to OutSeq items (58 of 80, 72.5%; e.g., Fig 3B), a significant proportion showed selectivity for InSeq items (22 of 80, 27.5%; e.g., Fig 3A). Here, we extend these findings by providing evidence that this form of nonspatial sequence coding was not evenly distributed along the four sections of the mediolateral/proximodistal axis from which we recorded.

Using multiple measures, we found that the strength of sequence coding varied across sections, and was highest in intermediate CA1 (section 2; Fig 3C-E). First, we examined the magnitude of sequence coding across all recorded cells per section by analyzing each cell's *t* ratio on the InSeq vs OutSeq test (converted to *F* ratios to be consistent with Allen et al., 2016). This primary analysis confirmed a significant difference across sections ($F_{(3, 709)} = 3.365$, $p = 0.0183$), with values significantly higher in section 2 than sections 1, 3, or 4 ($t_{2vs1\ (709)} = 2.518$, $p < 0.05$; $t_{2vs3\ (709)} = 2.305$, $p < 0.05$; $t_{2vs4\ (709)} = 2.563$, $p < 0.05$; Fig 3C). Then, we examined whether the same pattern was observed when our analyses focused exclusively on sequence cells (the cells with a significant *t* ratio on InSeq vs OutSeq comparison). Specifically, we focused on examining whether the proportion of sequence cells (normalized to the number of cells recorded in each sections; Fig 3D) and their sequential information content values (an indicator of how much information a given cell provides about the InSeq/OutSeq status of trials; Allen et al., 2016; Fig 3E) varied across sections. Despite the associated reduction in sample size (the overall incidence of sequence cells is relatively low; ~11% of cells), comparable distributions with a peak in section 2 were observed with these secondary analyses. The sequential content analysis showed a significant effect across sections ($F_{(3, 68)} = 8.510$, $p < 0.0001$; $t_{2vs1\ (68)} = 3.978$, $p < 0.05$; $t_{2vs3\ (68)} = 1.876$, ns ; $t_{2vs4\ (68)} = 4.087$, $p < 0.05$; Fig 3E), but the results of the proportion analysis were more mixed: the G-test did not reach significance here ($G_{3,\ N = 80} = 6.022$, $p = 0.1105$), but did when only including data from the first session (Well-Trained session only: $G_{3,\ N = 42} = 9.832$, $p = 0.02$; see below and Fig 3D).

Additional observations suggest this distribution was generally consistent across animals and cell types. For instance, we observed high proportions of sequence cells in section 2 in most (4/5) animals (see table 1), as well as when excluding the rat with the highest number of cells (proportions across sections without Rat 2: 0.09, 0.17, 0.09, 0.10) or the rat with the highest number of sequence cells (proportions without Rat 5: 0.07, 0.10, 0.05, 0.07), and when examining the distribution of sequence cell subtypes across sections (e.g., general vs conjunctive sequence cells, pyramidal vs interneurons; data not shown).

Due to the overall low incidence of sequence cells, the findings presented so far combined data from three separate sessions per animal to maximize sampling. Although most tetrodes were moved slightly after each session (in an attempt to maximize cell yield) and most sessions were separated by more than one day, this pooling raises the possibility that some cells may have been counted more than once. To account for this potential confound, we performed the same analyses including data from only one session per animal (Well-Trained session). We found comparable mean effect sizes (see gray bars in Fig 3C-E) though, as expected given the reduced sample size, the statistics were weaker. For instance, the ANOVA on the magnitude of sequence cell coding now had a p value of 0.06 ($F_{(3, 270)} = 2.468$, $p = 0.0624$; Fig 3C), the ANOVA on the sequential information content did not reach significance ($F_{(3, 37)} = 1.575$, $p = 0.2117$) but, interestingly, the G-test showed a significant difference in the proportion of sequence cells across sections (Well-Trained session only: $G_{3, N = 42} = 9.832$, $p = 0.020$; cf., all three sessions: $G_{3, N = 80} = 6.022$, $p = 0.1105$). The observation that the same pattern is visible in the data from a single session makes it unlikely that our results are primarily driven by the repeated inclusion of a small subset of sequence cells across sessions.

Overall, these findings are consistent with other reports showing that nonspatial information processing is not evenly distributed along the proximodistal axis of CA1, including studies showing that odor or object information is more strongly represented in distal CA1 than in proximal CA1 (Ito and Schuman, 2012; Nakamura et al., 2013; Igarashi et al., 2014b). Our findings add to these studies by suggesting that functional dissociations may also extend to intermediate CA1, a region those previous reports did not specifically examine.

Spatial coding showed a different distribution compared to nonspatial sequence coding

Although spatial processing is not critical to performance of the odor sequence memory task, rats were required to run to the back of the apparatus to begin the next sequence presentation (see Fig 1A). This requirement, combined with occasional exploration of the environment, provided

sufficient sampling to perform basic analyses of the spatial coding properties of individual neurons. Therefore, using the same set of animals and tetrodes as above, we were able to examine how spatial coding was distributed along the same CA1 axis.

Among the 713 recorded neurons, we found 257 units (36.0%) that showed firing to specific locations within the maze (place cells; see examples in Fig 4A). Our main finding is that the proportions of place cells across the four sections were significantly different than that of sequence cells (two-factor *G*-test: $G_{3,\ N = 337} = 9.457$, $p = 0.0240$). In fact, in contrast to the distribution of sequence cells reported above, the proportion of place cells increased toward proximal CA1 (Fig 4B). These observations were supported by *G*-tests, which showed that the proportion of place cells was significantly different across sections ($G_{3,\ N = 257} = 22.235$, $p = 0.0001$). Note that this effect was primarily driven by place cells with a single place field, as few cells had multiple place fields and their distribution was consistent across the four sections (<10%). We then explored the spatial information content provided by place cells across the four sections. We limited our analysis to putative pyramidal neurons with place fields on the runway (86 of 257; 33%), the section of the maze in which the animals' behavior, speed, and sampling were most consistent. Although the difference in values across sections did not reach significance ($F_{(3,82)} = 1.509$, $p = 0.2184$), high spatial information content values were observed in proximal CA1, which sharply contrasts with the pattern observed with sequential information content (compare Fig 4C with Fig 3E). Notably, we re-ran these analyses using data from only one session per animal (Well-Trained session) to control for the possibility that some cells may have been counted more than once, artificially increasing statistical power. This possibility does not appear to be the case since this approach produced similar results (see gray bars in Fig 4B,C); specifically, the proportion of place cells across sections remained significantly different than expected by chance ($G_{3,\ N = 117} = 9.832$, $p = 0.02$) and the spatial information content values remained high toward proximal CA1 (although the ANOVA now reached significance, $F_{(3,\ 26)} = 3.357$, $p = 0.0340$, the linear trend did not, $p = 0.0760$).

Secondary analyses suggest that, though place fields were found across the three major maze components (odor port area, runway, and start area), a higher proportion was observed in the start area ($G_{2,\ N = 320} = 19.237$, $p < 0.0001$) and particularly in proximal CA1 (section 4; $G_{3,\ N = 137} = 14.984$, $p = 0.0018$; Fig 4D). Notably, we also found a subset of neurons that exhibited both sequence and spatial coding (45 of 713 units; 6.3%) and the prevalence of these cells also increased toward proximal CA1 ($G_{3,\ N = 45} = 10.84$, $p = 0.013$; Fig 4E).

Overall, although our nonspatial memory task was not optimally designed for evaluating spatial coding properties of hippocampal CA1 neurons, the present results suggest the prevalence of

spatial coding increases towards proximal CA1, a finding consistent with recent reports (Henriksen et al., 2010; Oliva et al., 2016). The present study extends these findings by demonstrating, using the same set of animals and electrodes, that spatial and nonspatial sequence coding are differentially distributed along the proximodistal axis of CA1.

DISCUSSION

Recent studies have indicated that the processing of spatial and nonspatial information is not uniformly distributed along the transverse (proximodistal) axis of CA1, with spatial information being preferentially represented in proximal CA1 (Henriksen et al., 2010; Oliva et al., 2016) and nonspatial information in distal CA1 (e.g., odors or objects; Burke et al., 2011; Ito and Schuman, 2012; Nakamura et al., 2013; Igarashi et al., 2014b). The main objective of the present study was to examine how sequence cells, which code for the temporal context in which events occurred (in this case, whether or not an odor was presented in the correct sequential order), were distributed along the same axis. There were three main possibilities for how this form of nonspatial sequence coding could be distributed: *(1)* it arises from ensembles representing nonspatial information and thus should be primarily clustered in the distal end of CA1, *(2)* it shares fundamental principles with spatial coding (e.g., spatiotemporal context representation) and thus should be primarily represented in the proximal end of CA1, or *(3)* it is associated with a different type of integration (or convergence of inputs) and thus should result in a different distribution than the previous two possibilities. Our findings support the third possibility. Specifically, we found that the strength of sequence cell coding significantly varied along the transverse axis of CA1, with a peak in intermediate CA1 (section 2). Notably, all measures (magnitude, prevalence, and sequential information content) were low in distal CA1 (section 1), a sector in which odor or object information was reported in previous studies (Ito and Schuman, 2012; Igarashi et al., 2014b). Importantly, this distribution was significantly different than that of place coding, which showed an increasing proportion of cells with place fields toward proximal CA1 (section 4). These results suggest that nonspatial sequence (temporal) coding is differentially distributed than item or spatial coding in CA1.

Our findings corroborate recent reports in the literature. For instance, we found that both types of cells (sequence cells and place cells) were observed across the transverse axis, but that there were significant variations in their prevalence and/or specificity along the axis. This finding is consistent with recent place cell studies sampling the full transverse axis of CA1. In a study in which animals performed a random foraging task, Henriksen and colleagues (2010) reported place cells across the proximodistal axis but that spatial precision increased toward proximal CA1 (measured as an increase in spatial information content). In another study, Igarashi and colleagues (2014b) recorded from CA1 cells during learning of an odor-place association. Of all cells with a place field at the odor port on the first day of training (which were observed in distal and proximal sectors), the spatial coding properties of proximal CA1 cells remained consistent throughout training, whereas distal CA1 cells gained odor modulation. Similarly, immediate early gene

expression was reported in both proximal and distal CA1 in animals performing odor or object recognition tasks, but the expression was significantly higher in distal CA1 (Ito and Schuman, 2012; Nakamura et al., 2013). These findings are consistent with our observations that proximal CA1 appears primarily involved in the processing of spatial information, whereas other sectors can process nonspatial information. The present study extends these previous findings by providing the first characterization of the distribution of sequence coding (spatial or nonspatial), as well as a direct comparison with the distribution of place cell coding. Our study also complements previous work examining the distribution of nonspatial information, which has primarily focused on odor or object recognition memory (Ito and Schuman, 2012; Nakamura et al., 2013), by examining this coding in intermediate CA1 (in addition to distal and proximal CA1) in a paradigm that requires subjects to remember temporal relations among events, a critical contribution of the hippocampus to episodic memory (Fortin et al., 2002; Allen and Fortin, 2013; Howard and Eichenbaum, 2015).

It is important to note that the present study was not originally designed to test this specific hypothesis, so a few limitations and alternative explanations should be considered. First, the placement of our tetrode array yielded a more limited sampling of distal CA1 than recent studies specifically intended to sample the full transverse axis (Henriksen et al., 2010; Igarashi et al., 2014b; Oliva et al., 2016). However, previous studies have shown nonspatial modulation in the section of distal CA1 from which we recorded (Ito and Schuman, 2012; Nakamura et al., 2013; Igarashi et al., 2014b); thus, had sequence coding been localized in the same region, our sampling should have been sufficient to detect it. The mediolateral orientation of our tetrode array also means that our sampling was not perfectly aligned with the transverse axis, such that distal and proximal CA1 were sampled at slightly different septo-temporal levels. Though this difference was small and unlikely to produce the observed pattern of results on its own, this possibility should be assessed in future studies. Second, our experimental paradigm made it difficult to directly contrast the distribution of item and of sequence coding, as both types of information are overlapping on most trials (i.e., a cell responding to odor B in ABCDE may be coding for “odor B” or for “odor B when presented InSeq”). In our previous study (Allen et al., 2016), we successfully confirmed the presence of odor-selective cells by focusing our analyses on subsets of trials in which the two types of information are decoupled (OutSeq probe trials), but the number of such cells was too small (n = 15) for a meaningful examination of their distribution. Third, due to the relatively low incidence of sequence cells (~11% of cells), we maximized our sample sizes by combining data from three sessions. Although most tetrodes were slightly moved after each session and most sessions were not recorded on consecutive days, a subset of the cells may have been counted more than once, which could have artificially increased statistical power. However, the fact that the

same patterns are also visible in the data from a single session makes it unlikely that our results are primarily driven by this potential confounding factor. Similarly, although the low incidence of sequence cells precludes a thorough analysis of their distribution in each animal, the observation of a high proportion of sequence cells in section 2 was generally consistent across animals. Fourth, although we have previously examined potential strategies and cognitive representations supporting performance of this task in rodents and humans (see Allen et al., 2014, 2015), including item-item associations (e.g., “B is followed by C”) or item-position associations (e.g., “C is the third item in the sequence”), the present study was not designed to link the use of a specific strategy with the distribution of sequence coding in CA1. This assessment would require new experiments in which neural activity is recorded while biasing the animals toward the use of distinct strategies using different versions of the task. Finally, our experimental design was not ideal for spatial mapping, as the primary task demands involved performing a complicated nonspatial task in a specific location. Most studies quantifying spatial coding properties do so as animals explore large two-dimensional environments, with no explicit memory requirements, to maximize sampling and homogeneity of behavior. Although our paradigm provided enough sampling to quantify place cell proportions, it limited our ability to provide a detailed characterization of spatial coding properties. This could explain why our spatial information content analyses did not show the linear increase from distal to proximal CA1 reported by others (Henriksen et al., 2010; our distribution was more similar to a step function).

This potential peak in sequence cell coding in intermediate CA1 may indicate this form of temporal context information requires a different type of integration than item or spatial information processing, and may reflect a key convergence of inputs necessary for sequence memory performance. A distinctive feature of intermediate CA1 is that it receives more balanced inputs from LEC and MEC (unlike distal and proximal regions which receive stronger inputs from LEC and MEC, respectively). Our original working hypothesis on the emergence of sequence cells in CA1 focused on functional interactions with LEC and CA3 (see Allen et al., 2016). Specifically, we proposed that sequence cells reflect a comparative process in CA1, determining whether incoming information from LEC (representing the currently presented item) and from CA3 (representing the predicted item based on stored representation of the sequence) is a match (item is “in sequence”) or a mismatch (item is “out of sequence”). The strong oscillations in the 20-40 Hz range observed when animals sampled the odors in the task (Allen et al., 2016) are consistent with CA1-LEC coupling (Igarashi et al., 2014b). However, the distribution of sequence cells observed here suggests that MEC input to CA1 may also play a key role, potentially providing a form of self-generated spatiotemporal signal contributing to task performance (e.g., Kraus et al., 2015). Such

CA1-MEC coupling may have occurred during theta oscillations (e.g., Henriksen et al., 2010), which were prevalent during task performance (stronger during running bouts, but also present during odor sampling).

It remains to be determined whether sequence cells are specific to CA1. Our recent collaborative results, using high-resolution BOLD fMRI in humans performing the same sequence memory task, revealed strong activity in all hippocampal subregions examined (CA3/DG, CA1, and subiculum) on the same contrast used to identify sequence cells (InSeq vs OutSeq trials; Boucquey et al., 2015, submitted). Although this finding indicates all subfields are strongly engaged in the task, the extent to which this activity reflects sequence cell coding in all subregions or distinct subregion-specific contributions remains unclear. It will be particularly important for future studies to shed light on task-relevant coding properties in regions CA3 and CA2. Several prominent computational models have suggested that the unique neural architecture of CA3 (high density of recurrent collaterals) is well suited for sequence coding (e.g., McNaughton and Morris, 1987; Levy, 1996; Lisman, 1999), which is consistent with our preliminary findings that CA3 inactivations during task performance impair learning of a novel sequence (Asem et al., 2016). Notably, a different form of nonspatial temporal coding was recently reported in CA3 as well as in CA1 (“time cells”; Salz et al., 2016). Recent studies also suggest a potential role for CA2 in temporal coding (Mankin et al., 2015). Notably, CA2 is located near proximal CA1 (where we recorded few sequence cells) and may provide a different form of temporal signal than that described here (i.e., the passage of time rather than sequence relationships among events).

In conclusion, sequence cell activity is consistent with a fundamental role of the hippocampus in supporting the integration of information about specific items or events with the spatial and temporal context in which they occurred, a function critical to episodic memory (Eichenbaum et al., 2012; Allen and Fortin, 2013; Howard and Eichenbaum, 2015; Knierim, 2015). The present study shows that the distribution of this coding in CA1 parallels the convergence of inputs from LEC and MEC; it is present throughout the proximodistal axis, but higher in intermediate CA1, suggesting this form of nonspatial sequence coding emerges from complex functional interactions among hippocampal and entorhinal subregions. Ongoing studies focusing on quantifying sequence coding in these subregions, as well as identifying the distinct contribution of specific projections within this network of structures, will be needed to further address this important issue.

REFERENCES

Allen TA, Fortin NJ. 2013. The evolution of episodic memory. PNAS, 110, 10379-86.

Allen TA, Morris AM, Mattfeld AT, Stark CEL, Fortin NJ. 2014. A sequence of events model of episodic memory shows parallels in rats and humans. Hippocampus, 24, 1178-88.

Allen TA, Morris AM, Stark SM, Fortin NJ, Stark CEL. 2015. Memory for sequences of events impaired in typical aging. Learning & Memory, 22, 138-48.

Allen TA, Salz DM, McKenzie S, Fortin NJ. 2016. Nonspatial sequence coding in CA1 neurons. J Neurosci, 36(5), 1547-63.

Asem JSA, Kassir MH, Mirza NFB, Chmielewski NN, Elias GA, Ng CW, Allen TA, Fortin NJ. 2016. Using DREADDs to compare the effects of inactivating CA3 versus the CA3-CA1 projection on the memory for sequences of events. Society for Neuroscience Abstracts (San Diego, CA).

Boucquey VK, Allen TA, Huffman DJ, Fortin NJ, Stark CEL. 2015. Hippocampal and medial prefrontal cortex show activity and functional connectivity during memory for sequences of events. Society for Neuroscience Abstracts (Chicago, IL).

Boucquey VK, Allen TA, Huffman DJ, Fortin NJ, Stark CEL (submitted) A cross-species sequence memory task reveals hippocampal and prefrontal cortex activity in humans. Hippocampus.

Burke SN, Maurer AP, Nematollahi S, Uprety AR, Wallace JL, Barnes CA. 2011. The influence of objects on place field expression and size in distal hippocampal CA1. Hippocampus, 21(7), 783-801.

Cappaert NLM, Van Strien NM, Witter MP. 2015. Hippocampal Formation: The Rat Nervous System (Paxinos G Ed), Elsevier, Amsterdam, The Netherlands, fourth ed.

Csicsvari J, Hirase H, Czurko A, Buzsaki G. 1998. Reliability and state dependence of pyramidal cell-interneuron synapses in the hippocampus: an ensemble approach in the behaving rat. Neuron, 21, 179 –89.

Csicsvari J, Hirase H, Czurko A, Mamiya A, Buzsaki G. 1999. Oscillatory coupling of hippocampal pyramidal cells and interneurons in the behaving rat. J Neurosci, 19, 274 –87.

Deshmukh SS, Knierim JJ. 2011. Representation of non-spatial and spatial information in the lateral entorhinal cortex. Front Behav Neurosci, 5, 69.

Eichenbaum HB, Sauvage M, Fortin NJ, Komorowski R, Lipton P. 2012. Towards a functional organization of episodic memory in the medial temporal lobe. Neurosci Biobehav Rev, 36(7), 1597–1608.

Fortin NJ, Agster KL, Eichenbaum HB. 2002. Critical role of the hippocampus in memory for sequences of events. Nature Neuroscience, 5(5), 458–62.

Hafting T, Fyhn M, Molden S, Moser MB, Moser EI. 2005. Microstructure of a spatial map in the entorhinal cortex. Nature, 436(7052), 801-6.

Hargreaves EL, Rao G, Lee I, Knierim JJ. 2005. Major dissociation between medial and lateral entorhinal input to dorsal hippocampus. Science, 308(5729), 1792-4.

Hartzell AL, Burke SN, Hoang LT, Lister JP, Rodriguez CN, Barnes CA. 2013. Transcription of the immediate-early gene *Arc* in CA1 of the hippocampus reveals activity differences along the proximodistal axis that are attenuated by advanced age. J Neurosci, 33(8), 3424-33.

Henriksen EJ, Colgin LL, Barnes CA, Witter MP, Moser MB, Moser EI. 2010. Spatial representation along the proximodistal axis of CA1. Neuron, 68(1), 127-37.

Honda Y, Sasaki H, Umitsu Y,Ishizuka N. 2012. Zonal distribution of perforant path cells in layer III of the entorhinal area projecting to CA1 and subiculum in the rat. Neuroscience Res, 74, 200-209.

Howard MW, Eichenbaum HB.2015. Time and space in the hippocampus. Brain Research, 1621, 345–54.

Igarashi KM, Ito HT, Moser EI, Moser MB. 2014a. Functional diversity along the transverse axis of hippocampal area CA1. FEBS Lett, 588(15), 2470-6.

Igarashi KM, Lu L, Colgin LL, Moser MB, Moser EI. 2014b. Coordination of entorhinal-hippocampal ensemble activity during associative learning. Nature, 510(7503), 143-7.

Ito HT, Schuman EM. 2012. Functional division of hippocampal area CA1 via modulatory gating of entorhinal cortical inputs. Hippocampus, 22(2), 372-87.

Knierim, JJ 2015. The hippocampus. Current Biology, 25(23), R1116–R1121.

Knierim JJ, Lee I, Hargreaves EL. 2006. Hippocampal place cells: parallel input streams, subregional processing, and implications for episodic memory. Hippocampus, 16(9), 755-64.

Kraus BJ, Brandon MP, Robinson RJ, Connerney MA, Hasselmo ME, Eichenbaum HB. 2015. During running in place, grid cells integrate elapsed time and distance run. Neuron, 88(3), 578–589.

Levy WB. 1996. A sequence predicting CA3 is a flexible associator that learns and uses context to solve hippocampal-like tasks. Hippocampus, 6, 579 –90.

Lisman JE. 1999. Relating hippocampal circuitry to function: recall of memory sequences by reciprocal dentate-CA3 interactions. Neuron, 22, 233–42.

Lu L, Igarashi KM, Witter MP, Moser EI, Moser MB. 2015. Topography of place maps along the CA3-to-CA2 Axis of the hippocampus. Neuron, 87(5), 1078-92.

MacDonald CJ, Carrow S, Place R, Eichenbaum H. 2013. Distinct hippocampal time cell sequences represent odor memories in immobilized rats. J Neurosci, 33, 14607–16.

MacDonald CJ, Lepage KQ, Eden UT, Eichenbaum H. 2011. Hippocampal "time cells" bridge the gap in memory for discontiguous events. Neuron, 71(4), 737-49.

Mankin EA, Diehl GW, Sparks FT, Leutgeb S, Leutgeb JK. 2015. Hippocampal CA2 activity patterns change over time to a larger extent than between spatial contexts. Neuron, 85, 190–201.

McKenzie S, Robinson NT, Herrera L, Churchill JC, Eichenbaum H. 2013. Learning causes reorganization of neuronal firing patterns to represent related experiences within a hippocampal schema. J Neurosci, 33, 10243–56.

McNaughton BL, Morris RGM. 1987. Hippocampal synaptic enhancement and information storage within a distributed memory system. Trends Neurosci, 10(10), 408–15.

Mizuseki K, Buzsaki G. 2013. Preconfigured, skewed distribution of firing rates in the hippocampus and entorhinal cortex. Cell Reports, 4, 1010–21.

Naber PA, Lopes da Silva FH, Witter MP. 2001. Reciprocal connections between the entorhinal cortex and hippocampal fields CA1 and the subiculum are in register with the projections from CA1 to the subiculum. Hippocampus, 11(2), 99-104.

Nakamura NH, Flasbeck V, Maingret N, Kitsukawa T, Sauvage MM. 2013. Proximodistal segregation of nonspatial information in CA3: Preferential recruitment of a proximal CA3-distal CA1 network in nonspatial recognition memory. J Neurosci, 33(28), 11506-14.

Nakazawa Y, Pevzner A, Tanaka KZ, Wiltgen BJ. 2016. Memory retrieval along the proximodistal axis of CA1. Hippocampus, 26(9), 1140-8.

Neunuebel JP, Knierim JJ. 2014. CA3 retrieves coherent representations from degraded input: direct evidence for CA3 pattern completion and dentate gyrus pattern separation. Neuron, 81, 416–27.

Oliva A, Fernández-Ruiz A, Buzsáki G, Berényi A. 2016. Spatial coding and physiological properties of hippocampal neurons in the Cornu Ammonis subregions. Hippocampus, 26(12), 1593-1607.

Salz DM, Tiganj Z, Khasnabish S, Kohley A, Sheehan D, Howard MW, Eichenbaum HB. 2016. Time cells in hippocampal area CA3. J Neurosci, 36, 7476–84.

Sargolini F, Fyhn M, Hafting T, McNaughton BL, Witter MP, Moser MB, Moser EI. 2006. Conjunctive representation of position, direction, and velocity in entorhinal cortex. Science, 312(5774), 758-62.

Skaggs WE, McNaughton BL, Gothard KM, Markus EJ. 1993. An information-theoretic approach to deciphering the hippocampal code. Neural Inf Process Syst, 5, 1030 –7.

Sokal RR, Rohlf FJ. 1995. Biometry: The principles and practice of statistics in biological research. New York: W.H. Freeman.

Solstad T, Boccara CN, Kropff E, Moser MB, Moser EI. 2008. Representation of geometric borders in the entorhinal cortex. Science, 322(5909), 1865-8.

Witter MP, Wouterlood FG, Naber PA, Van Haeften T. 2000. Anatomical organization of the parahippocampal-hippocampal network. Ann N Y Acad Sci, 911, 1-24.

Wood ER, Dudchenko PA, Eichenbaum H. 1999. The global record of memory in hippocampal neuronal activity. Nature, 397(6720), 613-6.

Rat ID	Section							
	1		2		3		4	
	# cells	Prop.	# cells	Prop.	# cells	Prop.	# cells	Prop.
1	2/38	0.05	8/60	0.13	1/11	0.09	8/64	0.12
2	5/47	0.11	0/24	0	5/57	0.09	3/62	0.05
3	1/2	-	2/11	0.18	1/17	0.06	1/14	0.07
4	0/24	0	8/82	0.10	0/45	0	1/28	0.04
5	6/34	0.18	18/56	0.32	7/23	0.30	3/14	0.21

Table 1. Distribution of sequence cells across the CA1 transverse axis for each animal. While the numbers are relatively small when broken down per animal, high proportions of sequence cells in section 2 (intermediate CA1) are observed in most animals. Note that proportions are normalized to the number of recorded cells for the corresponding animal and section (proportions are only shown for sections with at least 10 recorded cells). Note that Rat 3 only provided data from one session as his headstage subsequently became defective.

FIGURE CAPTIONS

Figure 1. Sequence memory task design and procedures. Neural activity was recorded in dorsal CA1 as rats performed a nonspatial sequence memory task that shows strong behavioral parallels in rats and humans (Allen et al., 2014). **A,** Apparatus and behavioral procedures. The odor sequence memory task (panel B) was administered in a large apparatus separated in discrete areas (odor port area, runway, start area). For each sequence presentation, rats were required to: (1) run down the central runway toward the odor port area, (2) sample the sequence of odors in the port and identify each item as "in sequence" or "out of sequence," (3) run down the central runway to return to the start area, and (4) await the tone signaling that they could initiate the next sequence trial. Inset shows the automated odor delivery system capable of presenting distinct odors in the same odor port. **B,** Sequence memory task design. The task involves repeated presentations of sequences of odors in a single odor port and requires subjects to determine whether each item is presented in its correct sequence position ("in sequence," or InSeq; e.g., AB<u>C</u>…) or in the wrong sequence position ("out of sequence," or OutSeq; e.g., AB<u>D</u>…). Rats initiated each odor presentation by a nosepoke and identified InSeq or OutSeq items by how long they maintained their nosepoke response (holding until the signal, or ≥1.2s, for InSeq items; withdrawing before the signal for OutSeq items). Approximately half of the presentations included all items InSeq and the other half contained one item OutSeq. A small water reward was delivered just below the odor port after each correct nosepoke response (InSeq or OutSeq). A large water reward was given in the start area (on the other side of the apparatus) when rats correctly identified all five items of a sequence. If the rat committed an error, no water reward was given and the rat was required to return the start area and wait for the sound indicating the next odor sequence can now be presented.

Figure 2. Tetrode placements along the dorsal CA1 transverse axis. Tetrodes were evenly divided into four sections along the mediolateral axis of CA1, which was used as an approximation for the transverse/proximodistal axis (section 1: distal CA1; section 4: proximal CA1). The sample coronal slice shows example tetrode tip locations along the axis (red circles) as well as an approximation of the distal and proximal borders of CA1 (solid black lines).

Figure 3. Nonspatial sequence coding is not uniformly distributed along the CA1 transverse axis and peaks in intermediate CA1. A-B, Example sequence cells recorded in dorsal CA1 (Allen et al., 2016). Sequence cells are neurons that fire differentially to presented odors depending on the temporal context: in this case, whether they were presented "in sequence" (InSeq) or "out of sequence" (OutSeq). Note that this activity is observed while the animals' location and behavior

remains constant. The majority of sequence cells show increased firing to OutSeq items (**B**), but a significant proportion also displays the opposite pattern (**A**). Rasters (*top*) display spikes (ticks) and odor-sampling periods (shading) on individual trials. Perievent time histograms (*bottom*) show mean firing rates across all trials (±SEM), binned over 50 ms with minimal smoothing. Note that rasters display equivalent numbers of InSeq and OutSeq trials for clarity, but that histograms and statistical analyses included all trials with odor-sampling periods of 500 ms (*t*-tests performed on two 250 ms bins preceding port withdrawal). **C-E**, The strength of sequence cell coding varied across sections, with higher values observed in intermediate CA1 (section 2). To maximize sample sizes, analyses were performed on data collapsed across three separate sessions for each animal (black bars), but results from a single session show similar patterns (Well-Trained session; gray bars). **C**, Magnitude of sequence coding (*t* ratios of all recorded cells on InSeq vs OutSeq comparison, converted to *F* ratios) was significantly different across sections (one-way ANOVA), with posthoc tests showing higher values in section 2 than other sections. **D**, Proportion of recorded cells in each section that met statistical criterion for sequence cells (significant *t*-test on InSeq vs OutSeq comparison). **E**, Sequential information content of sequence cells was also significantly different across sections (one-way ANOVA on log-transformed scores, with posthoc tests showing significantly higher values in section 2 than 1 or 4). Note that the same pattern of results was obtained when the two highest information content values in section 2 were excluded from the analysis, indicating this effect was not driven by a few large data points. Gray circles represent information content values for all sequence cells in the present study. Error bars indicate ± 1 SEM. A*, significant ANOVA; *, significant *t*-test (corrected for the number of comparisons performed).

Figure 4. Spatial coding shows a different distribution along the CA1 transverse axis than nonspatial sequence coding. A, Example place cells recorded along the transverse axis of dorsal CA1 during performance of the sequence memory task. Color bars indicate mean firing rates in Hz for each rate map. **B-E**, The prevalence of place cell coding significantly varied across sections (*G*-tests), with higher proportions observed toward proximal CA1 (section 4), a distribution significantly different than that of sequence cells (two-factor *G*-test between data in panel 3D and 4B; G^{SvsP}). To maximize sample sizes, analyses were performed on data collapsed across three separate sessions for each animal (black bars), but results from a single session show similar patterns (Well-Trained session; gray bars in panels B and C). **B**, Proportion of recorded cells in each section that met the criterion for place cells. **C**, Spatial information content of place cells did not significantly vary across sections (one-way ANOVA), but the distribution is noticeably different than that observed with sequential information content (compare with Fig 3E). Note that this

analysis was limited to putative pyramidal neurons with place fields on the runway (n = 86), to maximize consistency in the animals' behavior, speed, and sampling. Gray circles represent information content values of all place cells in the present study. **D**, Distribution of place cells across sections and maze components (odor port area, runway, start area). **E**, Proportion of sequence cells in each section that also met the criterion for place cells. Error bars indicate ± 1 SEM. SIC, spatial information content. *G**, significant *G*-test. G^{SvsP}, significant two-factor *G*-test (sequence cell distribution vs place cell distribution).

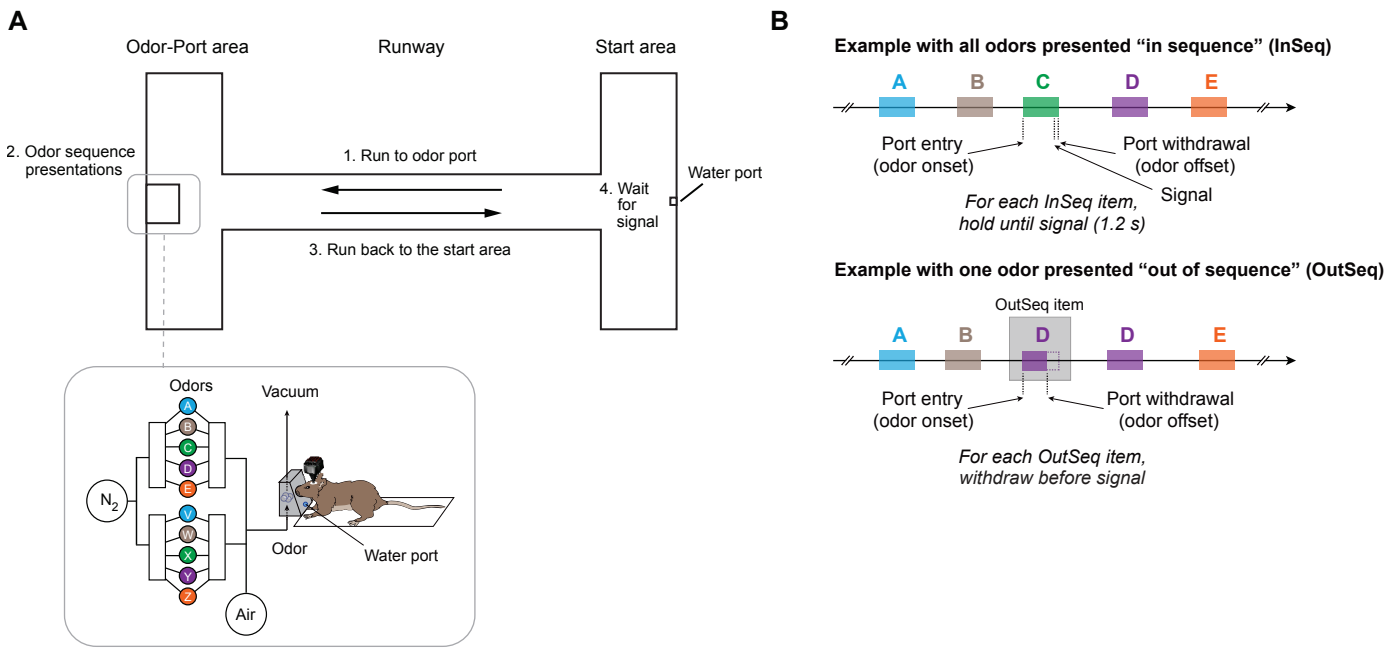

Figure 1. Sequence memory task design and procedures. Neural activity was recorded in dorsal CA1 as rats performed a nonspatial sequence memory task that shows strong behavioral parallels in rats and humans (Allen et al., 2014). Neural activity was recorded in dorsal CA1 as rats performed a nonspatial sequence memory task that shows strong behavioral parallels in rats and humans (Allen et al., 2014). **A**, Apparatus and behavioral procedures. The odor sequence memory task (panel B) was administered in a large apparatus separated in discrete areas (odor-port area, runway, start area). For each sequence presentation, rats were required to: (1) run down the central runway toward the odor-port area, (2) sample the sequence of odors in the port and identify each item as "in sequence" or "out of sequence," (3) run down the central runway to return to the start area, and (4) await the tone signaling that they could initiate the next sequence trial. Inset shows the automated odor delivery system capable of presenting distinct odors in the same odor port. **B**, Sequence memory task design. The task involves repeated presentations of sequences of odors in a single odor port and requires subjects to determine whether each item is presented in its correct sequence position ("in sequence," or InSeq; e.g., AB<u>C</u>…) or in the wrong sequence position ("out of sequence," or OutSeq; e.g., AB<u>D</u>…). Rats initiated each odor presentation by a nosepoke and identified InSeq or OutSeq items by how long they maintained their nosepoke response (holding until the signal, or ≥1.2s, for InSeq items; withdrawing before the signal for OutSeq items). Approximately half of the presentations included all items InSeq and the other half contained one item OutSeq. A small water reward was delivered just below the odor port after each correct nosepoke response (InSeq or OutSeq). A large water reward was given in the start area (on the other side of the apparatus) when rats correctly identified all five items of a sequence. If the rat committed an error, no water reward was given and the rat was required to return the start area and wait for the sound indicating the next odor sequence can now be presented.

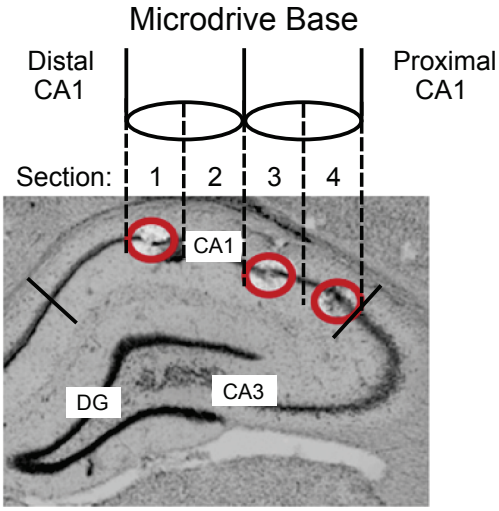

Figure 2. Tetrode placements along the dorsal CA1 transverse axis. Tetrodes were evenly divided into four sections along the mediolateral axis of CA1, which was used as an approximation for the transverse/proximodistal axis (section 1: distal CA1; section 4: proximal CA1). The sample coronal slice shows example tetrode tip locations along the axis (red circles) as well as an approximation of the distal and proximal borders of CA1 (solid black lines).

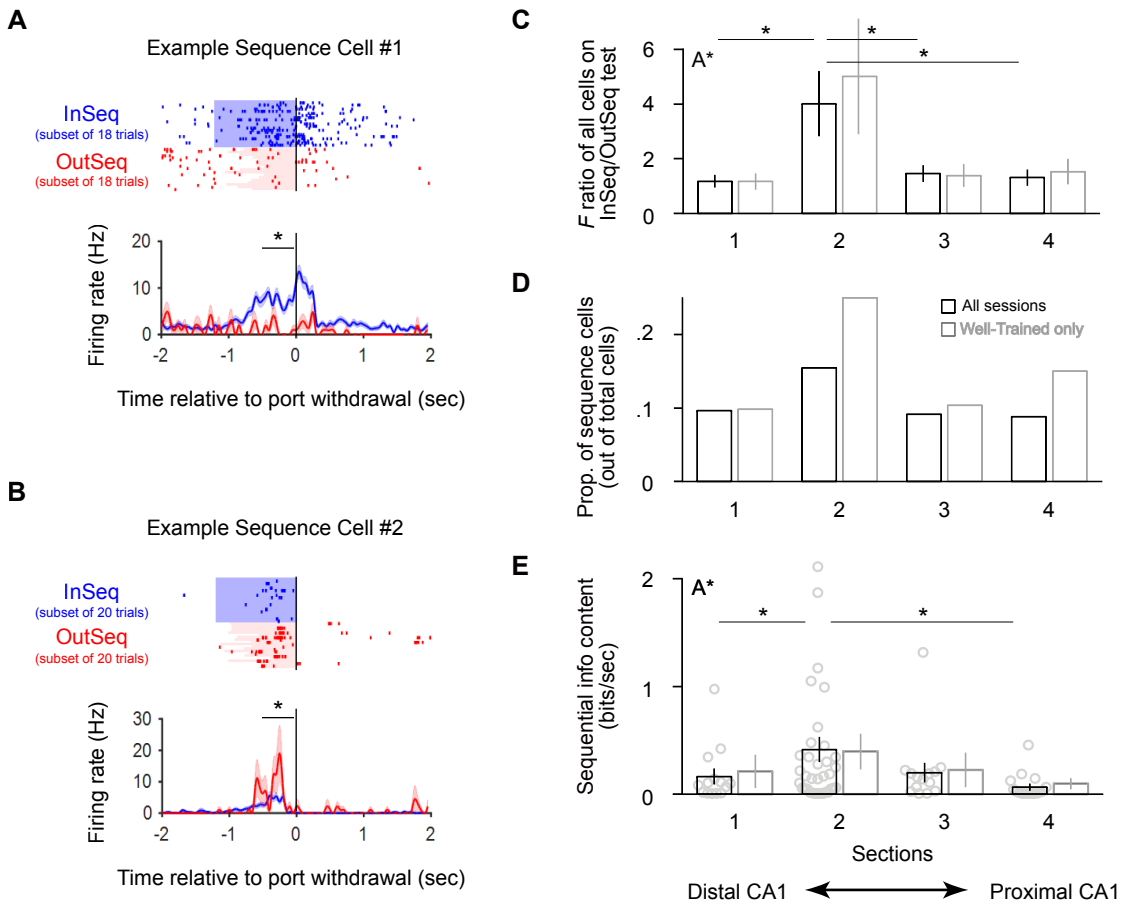

Figure 3. Nonspatial sequence coding is not uniformly distributed along the CA1 transverse axis and peaks in intermediate CA1. A-B, Example sequence cells recorded in dorsal CA1 (Allen et al., 2016). Sequence cells are neurons that fire differentially to presented odors depending on the temporal context: in this case, whether they were presented "in sequence" (InSeq) or "out of sequence" (OutSeq). Note that this activity is observed while the animals' location and behavior remains constant. The majority of sequence cells show increased firing to OutSeq items (**B**), but a significant proportion also displays the opposite pattern (**A**). Rasters (top) display spikes (ticks) and odor-sampling periods (shading) on individual trials. Perievent time histograms (bottom) show mean firing rates across all trials (±SEM), binned over 50 ms with minimal smoothing. Note that rasters display equivalent numbers of InSeq and OutSeq trials for clarity, but that histograms and statistical analyses included all trials with odor-sampling periods of 500 ms (t-tests performed on two 250 ms bins preceding port withdrawal). **C-E**, The strength of sequence cell coding varied across sections, with higher values observed in intermediate CA1 (section 2). To maximize sample sizes, analyses were performed on data collapsed across three separate sessions for each animal (black bars), but results from a single session show similar patterns (Well-Trained session; gray bars). **C**, Magnitude of sequence coding (t ratios of all recorded cells on InSeq vs OutSeq comparison, converted to F ratios) was significantly different across sections (one-way ANOVA), with posthoc tests showing higher values in section 2 than other sections. **D**, Proportion of recorded cells in each section that met statistical criterion for sequence cells (significant t-test on InSeq vs OutSeq comparison). **E**, Sequential information content of sequence cells was also significantly different across sections (one-way ANOVA on log-transformed scores, with posthoc tests showing significantly higher values in section 2 than 1 or 4). Note that the same pattern of results was obtained when the two highest information content values in section 2 were excluded from the analysis, indicating this effect was not driven by a few large data points. Gray circles represent information content values for all sequence cells in the present study. Error bars indicate ± 1 SEM. A*, significant ANOVA; *, significant t-test (corrected for the number of comparisons performed).

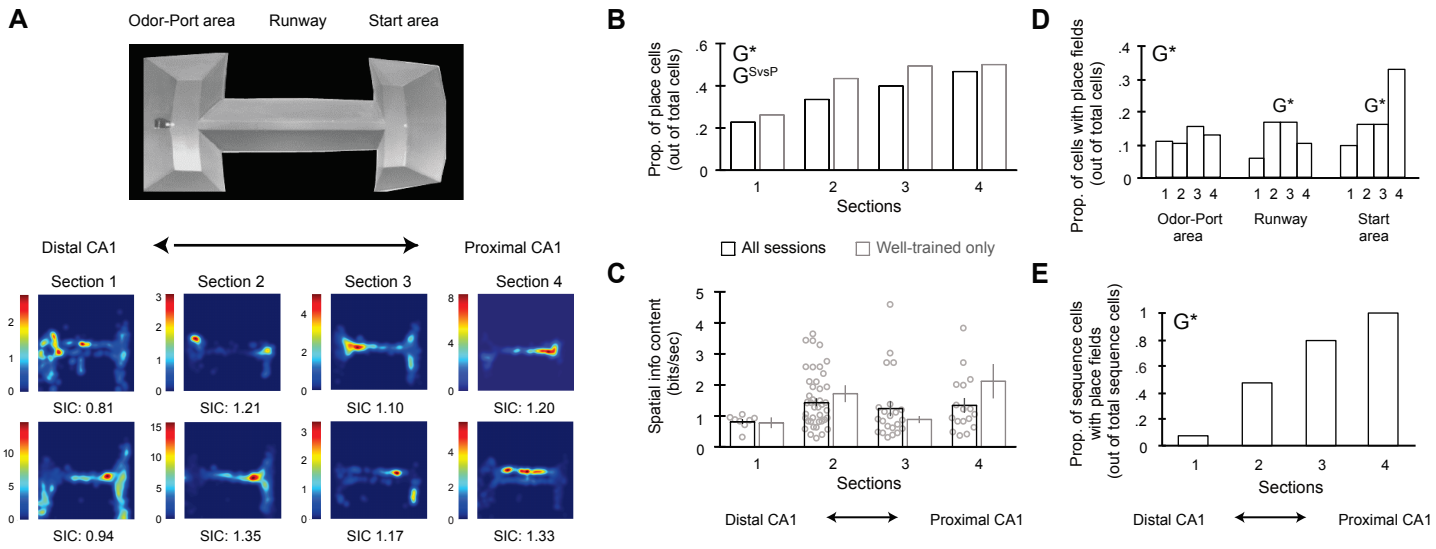

Figure 4. Spatial coding shows a different distribution along the CA1 transverse axis than nonspatial sequence coding. A, Example place cells recorded along the transverse axis of dorsal CA1 during performance of the sequence memory task. Color bars indicate mean firing rates in Hz for each rate map. **B-E**, The prevalence of place cell coding significantly varied across sections (G-tests), with higher proportions observed toward proximal CA1 (section 4), a distribution significantly different than that of sequence cells (two-factor G-test between data in panel 3D and 4B; G^{SvsP}). To maximize sample sizes, analyses were performed on data collapsed across three separate sessions for each animal (black bars), but results from a single session show similar patterns (Well-Trained session; gray bars in panels B and C). **B**, Proportion of recorded cells in each section that met the criterion for place cells. **C**, Spatial information content of place cells did not significantly vary across sections (one-way ANOVA), but the distribution is noticeably different than that observed with sequential information content (compare with Fig 3E). Note that this analysis was limited to putative pyramidal neurons with place fields on the runway (n = 86), to maximize consistency in the animals' behavior, speed, and sampling. Gray circles represent information content values of all place cells in the present study. **D**, Distribution of place cells across sections and maze components (odor-port area, runway, start area). **E**, Proportion of sequence cells in each section that also met the criterion for place cells. Error bars indicate ± 1 SEM. SIC, spatial information content. G*, significant G-test. G^{SvsP}, significant two-factor G-test (sequence cell distribution vs place cell distribution).